DOI 10.1007/s10946-024-10195-5
Journal of Russian Laser Research, Volume 45, Number 2, March, 2024

EFFECT OF PHOTON ADDITION ON GENUINE TRIPARTITE ENTANGLEMENT OF CONTINUOUS VARIABLE STATES

R. Sathiyabama and A. Basherrudin Mahmud Ahmed*

Department of Theoretical Physics, School of Physics, Madurai Kamaraj University Madurai, Tamil Nadu 625021, India

*Corresponding author e-mail: abmahmed @ gmail.com

Abstract

The enumeration of multipartite entanglement is an essential, yet challenging task in quantum information processing. A new measure for calculating genuine tripartite entanglement, called the concurrence fill (CF), has been added to the list of entanglement measures. In this article, we employ the CF to calculate the extent of entanglement present in the three-mode continuous variable states, such as the quasi-GHZ state and quasi-W state. The above mentioned states mimic their respective discrete variable states for moderate coherent strength, while for lower coherent strength, the states are far from possessing maximum entanglement. The photon addition in these states at the single mode and three-mode levels results in the states reaching their respective maximum amount of entanglement even for the lower coherent amplitude. In continuation, a nonlocal tripartite photon addition is implemented on a product three-mode coherent state, and the resultant state is shown to have W-type entanglement.

Keywords: coherent state, photon addition, concurrence fill, GHZ state, W state.

1. Introduction

Quantification of quantum correlations present in physical systems is of paramount interest in quantum information science. Entanglement is a kind of quantum correlation among spatially-separated physical systems and is regarded as a resource in protocols, such as quantum teleportation, metrology, and quantum cryptography [1]. Entanglement between two qubits can be calculated by employing concurrence, entanglement of formation [2], and the relative entropy of entanglement [3]. Beyond the two-qubit scenario, quantifying entanglement among multipartite systems has been challenging and an active area of research [4–10].

In 2000, Coffman et al. [11] coined the term tangle to represent the entanglement present in three qubits. At the tangle scale, the GHZ state reached its maximum, and the W state was shown to have a zero value. Eventually, to represent the entanglement among all three subsystems, a term called genuine tripartite entanglement was evolved. In the tripartite-qubit scenario, four specific classes exist: product, biseparable, GHZ, and W. All the tripartite qubits belong to any one of the above classes. In the case of biseparable and product states, at least one qubit is unshared from the other two qubits. In the GHZ and W states, all the subsystems are genuinely entangled. Hence, the genuine tripartite entanglement measure must assign zero values to the states falling in the product and biseparable classes, while nonzero values must be assigned to the GHZ and W class states. Based on the conditions imposed for genuine

Manuscript submitted by the authors in English on January 3, 2024.

tripartite entanglement, the tangle failed to become a genuine tripartite entanglement measure. Recently, a new measure of genuine three-qubit entanglement has been proposed [12]. This measure, known as the concurrence fill, is based on the quantification of a triangle's area formed by the square root of concurrence among the three bipartitions. The GHZ state attains the perfect one value, while the W state reaches 8/9. The success of this measure also induces similar attempts in the case of four-pure-qubit case [13].

The experimental feasibility of radiation states makes them attractive for the implementation of quantum information protocols [14]. A light field in the coherent state is a classical state possessing minimum uncertainty. Manipulation involving the photon addition [15] and subtraction [16] turn the coherent state into a nonclassical state. At the single-mode level, the extent of nonclassicality creation, using photonic operations, is known [17]. Extending to two modes, using a nonlocal operation with a photon creation operator on a product coherent state leads to entanglement between the two modes [18]. Here, the photon-added coherent states were mapped to qubits, and entanglement between the two qubits was calculated using concurrence.

In this article, we extend this approach to three modes and employ a trimodal nonlocal photon-addition operation on three product coherent states. The resultant state is genuinely entangled and evaluated using the CF measure.

The present work is organized as follows.

We discuss the genuine tripartite entanglement in Sec. 2 while, in Sec. 3, we examine the effects of the photon-addition operation on the tripartite continuous-variable (CV) states. Consequently, the genuine three-qubit entanglement present in well-known states, such as quasi-GHZ and quasi-W states, is calculated, and the impacts of the single-mode and three-mode photon additions on these states are also calculated. In Sec. 3.2, we describe the derivation of the CF due to the influence of nonlocal photon addition. Concluding remarks are given in Sec. 4.

2. Genuine Tripartite Entanglement Measure

In 2021, Xie et al. [12] introduced a novel method called the CF to measure the amount of entanglement present among three pure qubits. This method is based on Heron's formula for calculating the area of the concurrence triangle. The lengths of the three edges of this triangle correspond to the squared edges to the other concurrences. The area of this concurrence triangle serves as a genuine three-qubit entanglement measure for pure states. Consider three qubits, A, B, and C, which can be partitioned into $A|BC$, $B|AC$, and $C|AB$, respectively. The entanglement between these partitions can be evaluated, using concurrence. These concurrences are denoted as $\mathcal{C}^2_{A|BC}$, $\mathcal{C}^2_{B|CA}$, and $\mathcal{C}^2_{C|AB}$. Based on these concurrences, the CF is given as

$$F_{ABC} = \left[\frac{16}{3}\mathcal{Q}(\mathcal{Q}-\mathcal{C}^2_{A|BC})(\mathcal{Q}-\mathcal{C}^2_{B|AC})(\mathcal{Q}-\mathcal{C}^2_{C|AB})\right]^{1/4}, \tag{1}$$

where $\mathcal{Q}$ is the half perimeter and given as

$$\mathcal{Q} = \frac{1}{2}\left(\mathcal{C}^2_{A|BC}+\mathcal{C}^2_{B|AC}+\mathcal{C}^2_{C|AB}\right). \tag{2}$$

A factor of 16/3 ensures normalization. The CF is bounded between 0 and 1; $0 \le F_{ABC} \le 1$.

3. Tripartite CV States

CV states play a vital role in the implementation of quantum information protocols due to their laboratory readiness and efficient manipulation [19,20]. One of the implementation tactics is to map them as two-level systems – qubits [21]. This mapping of CV states into qubits facilitates implementation. The coherent state is the most well-known CV state. While the coherent state is classical, the superposition of coherent states offers the unique advantage of realizing Schrödinger cat states. Although any two coherent states are nonorthogonal, sufficient coherent strength will cause their overlap to vanish. At the two-mode level, all the maximum entangled Bell states are mapped and called the quasi-Bell states [22]. In the case of discrete variable (DV), the GHZ and W states are well-known forms of tripartite entanglement. The distinction between them becomes apparent, when one of the modes is traced over, leading to residual bipartite entanglement. In this scenario, the reduced GHZ state becomes separable, while the reduced W-state retains some degree of bipartite entanglement. Adesso et al. [23] extensively studied these states in the context of CV quantum information. The GHZ state in the CV regime is given as

$$|\psi\rangle_{\rm GHZ} = N_{\rm GHZ}\big[|\xi\rangle_a|\xi\rangle_b|\xi\rangle_c + |-\xi\rangle_a|-\xi\rangle_b|-\xi\rangle_c\big], \tag{3}$$

where $|\xi\rangle = e^{-|\xi|^2/2}\sum_{p=0}^{\infty}\frac{\xi^p}{\sqrt{p!}}|p\rangle$ is the coherent state. Using the coherent state, the quasi-W state can be expressed as

$$|\psi\rangle_W = N_W\left[|-\xi\rangle_a|\xi\rangle_b|\xi\rangle_c + |\xi\rangle_a|-\xi\rangle_b|\xi\rangle_c + |\xi\rangle_a|\xi\rangle_b|-\xi\rangle_c\right]. \tag{4}$$

The normalization constants are given by $N^2_{\rm GHZ} = 1/(2+2e^{-6|\xi|^2})$ and $N^2_W = 1/(3+6e^{-4|\xi|^2})$.

To map these states into the DV case, a two-dimensional basis, that consists of orthogonal qubits $|+\rangle$ and $|-\rangle$, is introduced. The orthogonal qubits are given as $|\pm\rangle = \frac{1}{\sqrt{2\pm 2e^{-2|\xi|^2}}}(|\xi\rangle \pm |-\xi\rangle)$. Using the above qubit encoding, we calculate the CF for the quasi-GHZ state and quasi-W state. The analytical expressions CF for both of the states read

$$F = \frac{4}{(2+2e^{-6|\xi|^2})^2}\left\{(1-e^{-4|\xi|^2})(1-e^{-8|\xi|^2})\right\} \qquad \text{(quasi-GHZ)}, \tag{5}$$

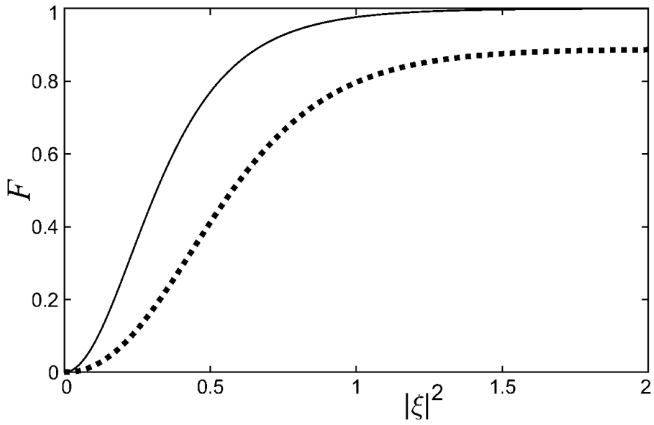

Fig. 1. Plots of the CF and optical strength $|\xi|^2$ for quasi-GHZ (the solid curve), and quasi-W (the dashed curve).

$$F = \frac{8(1-2e^{-4|\xi|^2}+e^{-8|\xi|^2})}{(3+6e^{-4|\xi|^2})^2} \qquad \text{(quasi-W)}. \tag{6}$$

In Fig. 1. we show the CFs of the quasi-GHZ and quasi-W states as a function of $|\xi|^2$. From Eqs. (5) and (6), it is evident that as $|\xi|^2$ increases, the CF of the quasi-GHZ state reaches 1, and the CF of the quasi-W state reaches 8/9. However, in the lower coherent strength regime, the quasi-GHZ and quasi-W states possess non-maximum entanglement in their respective regimes.

3.1. Local Photon Excitation as an Entanglement Enhancement

Various methods, such as the photon addition [15], photon subtraction [16], filtration [24], and truncation [25], have been employed to create robust nonclassical radiation states. Agarwal and Tara introduced single-mode photon-added coherent states (PACS), which were experimentally realized in 2004 [26]. Photon addition to the thermal state, called the photon-added thermal state, was also experimentally prepared in [27]. Extending to multimode cases, photon addition has been shown to introduce or enhance the correlations among the field modes. The normalized k PACSs are defined as $|\xi,k\rangle = \frac{(a^{\dagger k})|\xi\rangle}{\sqrt{\langle\xi|\hat{a}^k a^{\dagger k}|\xi\rangle}}$, where the overlap between the two states is $\langle\xi|a^k a^{\dagger k}|\xi\rangle = k!L_k(-|\xi|^2)$, and $L_k(x)$ is the Laguerre polynomial defined as $L_k(x) = \sum_{p=0}^{k} \frac{(-1)^p k! x^p}{(p!)^2(k-p)!}$. The overlap between the two states is helpful for the upcoming calculation $\langle\xi|a^k a^{\dagger k}|-\xi\rangle = e^{-2|\xi|^2} k!L_k(-|\xi|^2)$.

3.1.1. Single-Mode Photon Excitation

In 2009, Heng Mei Li et al. [28] calculated the degree of entanglement for the single-mode excited GHZ (SMEGHZ) state through the action of the creation operator on quasi-GHZ states. The quantification of entanglement, representing both the concurrence and violation of the CHSH inequality, was also assessed. The investigation of CHSH inequality violations in SMEGHZ states employed the formalism of the Wigner representation in the phase space, incorporating parity measurements and displacement operators. The authors proposed feasible schemes for generating SMEGHZ states.

Daoud et al. [29] focused on how the excitation of photons affects the monogamy property of quantum discord in tripartite coherent states of the GHZ type. The pairwise correlations are gauged using entropy-based quantum discord, and the augmentation of correlations is contingent upon the number of photon excitations. As the number of photon additions increases, so does the level of correlation. The SMEGHZ and single-mode excited W (SMEW) states can be acquired through the iterative utilization of the creation operator on the three-mode quasi-GHZ state and quasi-W state. These states are represented as follows:

$$|\psi\rangle_{\text{SMEGHZ}} = N_{\text{SMEGHZ}} \left[a^{\dagger k}(|\xi\rangle_a|\xi\rangle_b|\xi\rangle_c + |-\xi\rangle_a|-\xi\rangle_b|-\xi\rangle_c)\right], \tag{7}$$

where N_{SMEGHZ} is the normalization constant of SMEGHZ and can be calculated as

$$N^2_{\text{SMEGHZ}} = 1/[2 + 2s_k e^{-6|\xi|^2}]. \tag{8}$$

Also,

$$|\psi\rangle_{\text{SMEW}} = N_{\text{SMEW}} \left[a^{\dagger k}(|-\xi\rangle_a|\xi\rangle_b|\xi\rangle_c + |\xi\rangle_a|-\xi\rangle_b|\xi\rangle_c + |\xi\rangle_a|\xi\rangle_b|-\xi\rangle_c)\right], \tag{9}$$

where N_{SMEW} is the normalization constant of SMEW and can be computed as

$$N^2_{\text{SMEW}} = 1/[3 + 2e^{-4|\xi|^2}(1 + 2s_k)]. \tag{10}$$

Here, $s_k \equiv s_k(|\xi|^2) := \left[\frac{L_k(|\xi|^2)}{L_k(-|\xi|^2)}\right]$. Identification of photon-added coherent states $|\xi,k\rangle$ and $|-\xi,k\rangle$ as the foundation of a logical qubit is feasible only for greater coherence parameters ($\xi > 2$) because of

the nonorthogonality criterion. A qubit can be encoded, using coherent states. In fact, based on the encoding method, we construct a two-dimensional basis covered by orthogonal qubits $|+,k\rangle$ and $|-,k\rangle$,

$$|\pm,k\rangle = \frac{1}{\sqrt{2 \pm 2s_k e^{-2|\xi|^2}}}(|\xi,k\rangle \pm |-\xi,k\rangle). \tag{11}$$

The reduced formula for SMEGHZ and SMEW is calculated from Eq. (2), it reads

$$F = \left\{ \frac{16}{3} \left(\frac{\mathcal{C}_A^4 \mathcal{C}_B^4}{4} - \frac{\mathcal{C}_A^8}{16} \right) \right\}^{1/4}. \tag{12}$$

Analytically, $\mathcal{C}_A^4$, $\mathcal{C}_B^4$, and $\mathcal{C}_A^8$ can be calculated through the following determinant values.

The reduced determinant values of SMEGHZ are given as follows:

$$\det(\rho_A)_{\text{SMEGHZ}} = N_{\text{SMEGHZ}}^4 (1 - s_k^2 e^{-4|\xi|^2})(1 - e^{-8|\xi|^2}), \tag{13}$$

$$\det(\rho_B)_{\text{SMEGHZ}} = N_{\text{SMEGHZ}}^4 (1 - s_k^2 e^{-8|\xi|^2})(1 - e^{-4|\xi|^2}). \tag{14}$$

The reduced determinant values of SMEW state are given as follows:

$$\det(\rho_A)_{\text{SMEW}} = 2N_{\text{SMEW}}^4 (1 - s_k^2 e^{-4|\xi|^2})(1 - e^{-4|\xi|^2}), \tag{15}$$

$$\det(\rho_B)_{\text{SMEW}} = N_{\text{SMEW}}^4 \left(2 + e^{-8|\xi|^2}(1 + s_k + 3s_k^2) - e^{-4|\xi|^2}(3 + s_k + s_k^2) \right). \tag{16}$$

To observe the influence of single-mode photon excitation on the quasi-GHZ and quasi-W states, in Fig. 2, we plot the CF in Eq. (12) as a function of $|\xi|^2$ for different values of k. We note that the CF is sensitive and increases with increasing photon excitation k. From Figs. 2 a ,b, when $F = 0$, we can easily see that $|\xi| = 0$. The results show that the CF increases with increasing $|\xi|^2$ for a given parameter k. These results can be confirmed analytically in the above discussion. In other words, we can increase the CF of the SMEGHZ and SMEW states by repeated application of the photon creation operator.

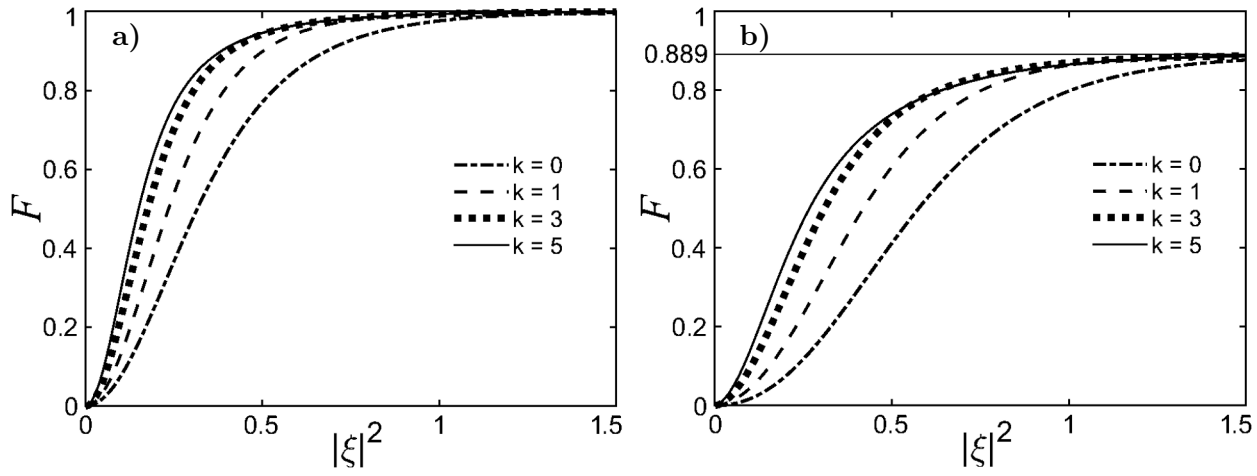

Fig. 2. The relation between the CF and optical strength $|\xi|^2$ for SMEGHZ (a) and SMEW (b). Here, $k = 0$ (dash-dotted curve), $k = 1$ (dashed curve), $k = 3$ (dotted curve), and $k = 5$ (solid curve).

3.1.2. Three-Mode Photon Excitations

Recently, Daoud et al. [30] explored three-mode excited quasi-GHZ by iteratively applying the photon added operator to the quasi-GHZ state. This study delves into the impact of this operation on the nonclassical and non-Gaussian behavior of the three-mode excited GHZ (TMEGHZ) state. These authors demonstrated that nonclassical properties can be enhanced in the TMEGHZ state as the photon number increases.

Based on the above study, we generate photon excited quasi-GHZ and quasi-W states through the repeated application of the creation operator. This process yields the TMEGHZ-type and three-mode excited W (TMEW) type states,

$$|\psi\rangle_{\rm TMEGHZ} = N_{\rm TMEGHZ}\left[a^{\dagger k}b^{\dagger k}c^{\dagger k}(|\xi\rangle_a|\xi\rangle_b|\xi\rangle_c + |-\xi\rangle_a|-\xi\rangle_b|-\xi\rangle_c)\right], \tag{17}$$

where $N_{\rm TMEGHZ}$ state is the normalization constant of TMEGHZ and can be calculated as

$$N^2_{\rm TMEGHZ} = 1/(2 + 2s_k^3 e^{-6|\xi|^2}). \tag{18}$$

Also,

$$|\psi\rangle_{\rm TMEW} = N_{\rm TMEW}\left[a^{\dagger k}b^{\dagger k}c^{\dagger k}(|-\xi\rangle_a|\xi\rangle_b|\xi\rangle_c + |\xi\rangle_a|-\xi\rangle_b|\xi\rangle_c + |\xi\rangle_a|\xi\rangle_b|-\xi\rangle_c)\right], \tag{19}$$

where $N_{\rm TMEW}$ state is the normalization constant of the TMEW and can be calculated as

$$N^2_{\rm TMEW} = 1/(3 + 6s_k^2 e^{-4|\xi|^2}). \tag{20}$$

The analytical expression of the CF for the TMEGHZ state reads

$$F = \frac{4}{(2 + 2s_k^3 e^{-6|\xi|^2})^2}\left\{1 - s_k^2 e^{-4|\xi|^2} - s_k^4 e^{-8|\xi|^2} + s_k^6 e^{-12|\xi|^2}\right\}. \tag{21}$$

The analytical expression of the CF for the TMEW state is

$$F = \frac{1}{(3 + 6s_k^2 e^{-4|\xi|^2})^2}\left(8 + 38s_k^4 e^{-8|\xi|^2} - 4s_k^6 e^{-12|\xi|^2} - 14s_k^2 e^{-4|\xi|^2}\right). \tag{22}$$

We use Eqs. (21) and (22) to discuss the CFs in the TMEGHZ and TMEW states. In Fig. 3 a, b, we show the CF as a function of $|\xi|^2$ for various values of k. In general, higher CF values correspond to

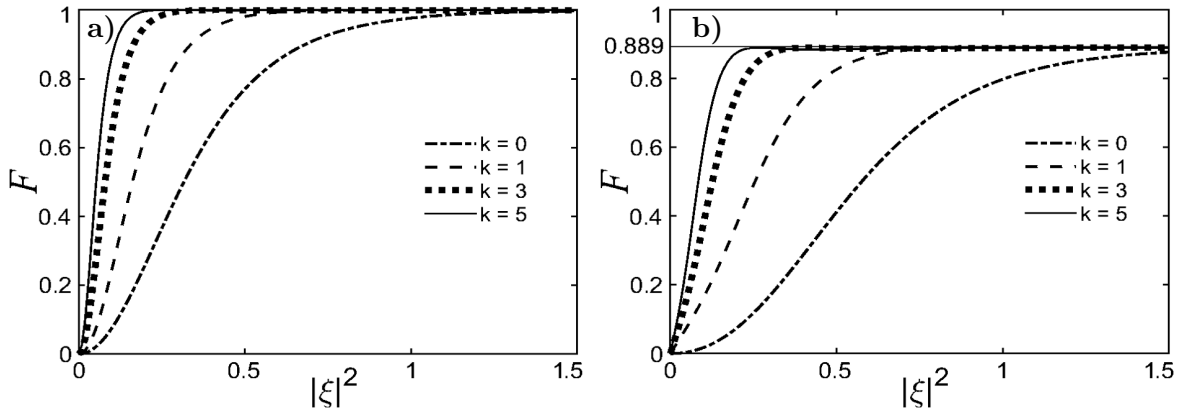

Fig. 3. Plots of the CF and optical strength $|\xi|^2$ for the TMEGHZ (a) and TMEW (b). Here, $k = 0$ (dash-dotted curve), $k = 1$ (dashed curve), $k = 3$ (dotted curve), and $k = 5$ (solid curve).

better genuine tripartite entanglement. We observe that the CFs of the TMEGHZ and TMEW states are greater than those of the SMEGHZ and SMEW states for smaller $|\xi|^2$. Furthermore, the maximum CFs are consistently equal to 1 and 0.889 in the TMEGHZ and TMEW, respectively. Additionally, for several values of k, the CF increases and reaches its maximum even for small values of $|\xi|^2$.

In Fig. 4, we illustrate the concurrence triangle, representing the area of CF for three states: the quasi-GHZ state (a), SMEGHZ state (b), and TMEGHZ state (c). Figure 4 explores the CF area while maintaining fixed coherent parameter values of 0.5. Figure 4 a shows that the concurrence triangle takes the form of an equilateral triangle, indicating that all three sides are of equal length. Notably, in the quasi-GHZ state (a), no photons are introduced, resulting in a minimum CF area compared to that of the other GHZ states.

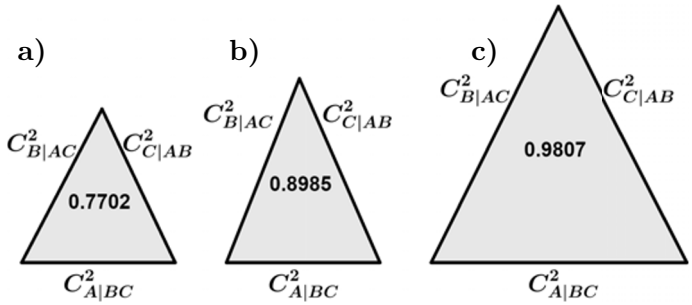

Fig. 4. Concurrence triangle representing the area of CF for the quasi-GHZ (a), SMEGHZ (b), and TMEGHZ (c) states.

In Fig. 4 b, an isosceles triangle is depicted, indicating that the two sides are equal, while one side differs due to the excitation of photons ($k = 1$) into the first mode of the quasi-GHZ state. Consequently, the CF area in Fig. 4 b is an intermediate between the quasi-GHZ and TMEGHZ states. Figure 4 c reveals an equilateral triangle, representing the TMEGHZ state, with all the sides being equal. Here, photons are added ($k = 1$) to all three modes in the quasi-GHZ states. Notably, the CF area is significantly closer to the maximum compared to the previous quasi-GHZ and SMEGHZ states.

In Fig. 5, we show the concurrence triangle, which represents the area for three states: the quasi-W state (a), the SMEW state (b), and the TMEW state (c). The purpose of Fig. 5 is to explore the CF area while maintaining a fixed coherent parameter value of 0.5. As shown in Fig. 5 a, the concurrence triangle takes the form of an equilateral triangle, indicating that all three sides are of equal length. Notably, in the quasi-W state (a), no photons are introduced, resulting in a minimum CF area compared to that of the other states. Transferring to Fig. 5 b, an isosceles triangle is observed, signifying that the two sides are equal, while one side differs due to the addition of photons to the first mode in the quasi-W state. Therefore, the CF area in Fig. 5 b is increased relative to that in the prior quasi-W state. Figure 5 c portrays an equilateral triangle, denoting three equal sides; in this scenario, photons are added to all three modes in the TMEW state. Compared with those in the previous quasi-W and SMEW states, the CF area in Fig. 5 c is nearly maximum.

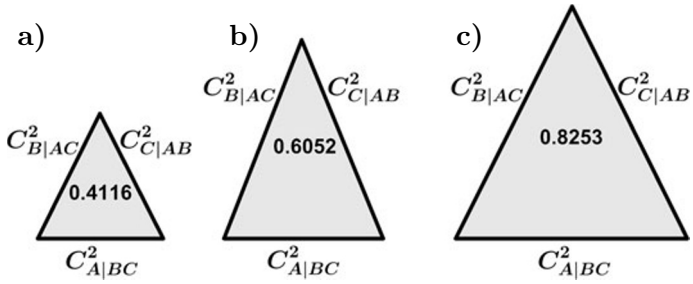

Fig. 5. Concurrence triangle representing the area of CF for the quasi-W (a), SMEW (b), and TMEW (c) states.

3.2. Creating Genuine Tripartite Entanglement Using the Nonlocal Photon Addition Operation

For multimode systems, quantum correlations can be improved by nonlocal operations. Nonlocal single and two photon addition operations on two-mode entangled states of light are generated by conditional

measurements for quantum lithography [31]. The created states are used as a resource for quantum information. Another important nonlocal second-order photon addition method for arbitrary two-mode states (NOON) was designed using Hong–Ou–Mandel interference [32]. Additionally, the improvement in the entanglement properties was investigated and the experimental feasibility of the generated states in terms of the phase properties was studied. The nonclassical correlations of nonlocal coherent photons with two-mode squeezed thermal states were studied in [33], which nonlocal photon addition operations enhanced the nonclassical correlations. The addition of multiple nonlocal photons to two-mode squeezed vacuum states was discussed in [34]. The nonlocal photon addition operation enhanced the degree of entanglement and the EPR correlations. Furthermore, the hierarchical quantum correlations of nonlocal multiple photons added to the thermal state were investigated in [35]. Additionally, nonlocal photons with bipartite coherent states were added and their properties were studied by [18]. These previous studies revealed that nonlocal photon addition enhances the quantum correlation. Here, we generate the nonlocal tripartite photon added coherent states (NLTPACS), using bosonic creation operator,

$$|\psi\rangle = a^{\dagger k} + b^{\dagger k} + c^{\dagger k}\left[N(|\xi\rangle_a|\xi\rangle_b|\xi\rangle_c)\right], \tag{23}$$

where N is the normalization constant of NLTPACS and can be calculated as

$$N = \frac{1}{\sqrt{3L_k(-|\xi|^2)k! + 6|\xi|^{2k}}}. \tag{24}$$

The orthogonal basis for the NLTPACS can be taken as follows:

$$|0\rangle = |\xi\rangle, |1\rangle = N_1\left[a^{\dagger k}|\xi\rangle - z_1|0\rangle\right]; \qquad z_1 = \xi^{*k}, \tag{25}$$

where $N_1 = [L_k(-|\xi|^2)k! - |\xi|^{2k}]^{-1/2}$. In terms of the two-qubit orthogonal computing basis, the state in Eq. (23) reads

$$|\psi\rangle = N\left[(3\alpha^k)|000\rangle + \frac{|001\rangle + |010\rangle + |100\rangle}{N_1}\right]. \tag{26}$$

The CF of NLTPACS is expressed as

$$F = \frac{8(L_k(-|\xi|^2)k! - |\xi|^{2k})^2}{[3(L_k(-|\xi|^2)k! + 2|\xi|^{2k})]^2}. \tag{27}$$

Figure 6 a illustrates the effect of nonlocal photon addition on the product coherent states. For the coherent parameter $\xi = 0$, the resultant state is $\frac{1}{\sqrt{3}}(|k\rangle|0\rangle|0\rangle + |0\rangle|k\rangle|0\rangle + |0\rangle|0\rangle|k\rangle)$. The CF of this W-type state is 8/9. For the nonzero coherent parameter case, the CF starts declining from the maximum. However, for larger k values, the state retains the maximum CF for sufficient coherent strength. This can be portrayed as the interplay between classical noise, i.e., coherent strength, and infused quantum noise through nonlocal photon addition. At $\xi = 0$, the state is a quantum-mechanical state composed of superposition of the number states $|k\rangle$ and $|0\rangle$. For nonzero coherence strength, the state can be viewed as nonlocal-operation-induced quantum noise imposed on the classical coherent state. The influence of the ratio of these two competing noises, nonlocal quantum noise versus classical coherent noise, on the CF is shown; the ratio is given as

$$\eta = \frac{\langle N\rangle_{\text{NLTPACS}} - 3|\xi|^2}{3|\xi|^2}.$$

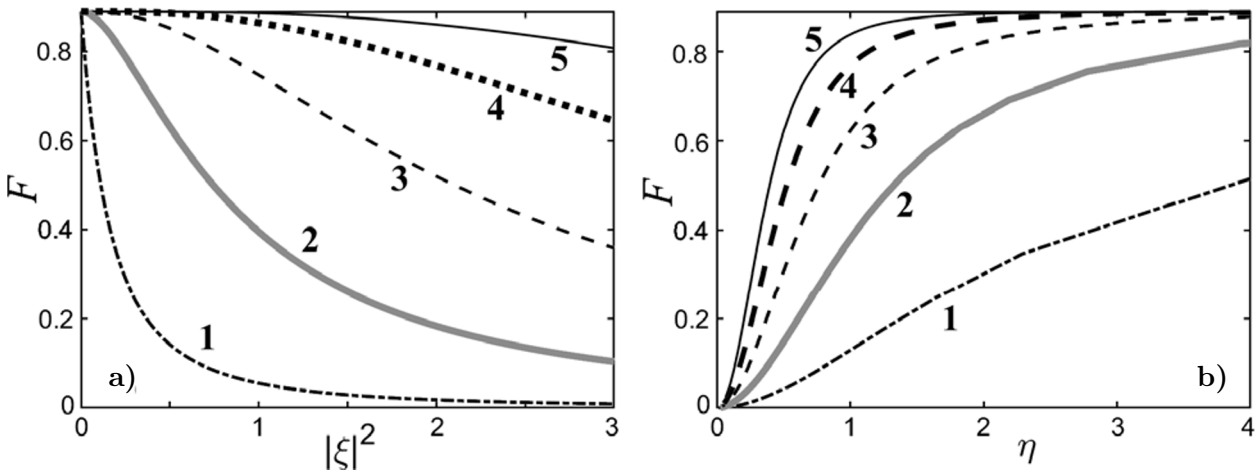

Fig. 6. CF and optical strength $|\xi|^2$ for NLTPACS (a) and the noise ratio η and CF (b) for different values of k written near curves.

Here, the term $3|\xi|^2$ represents the classical coherent noise. The numerator denotes the added nonlocal quantum noise, and the denominator represents the classical coherent noise. The behavior of the CF for the range of η is illustrated in Fig. 6 b. As the ratio tends to vanish, i.e., as the infused quantum noise is dominated by classical coherent noise, the CF goes to zero. From Fig. 6 b, it is inferred that the addition of each k photons follows its own trend. Even for the quadrupled ratio value ($\eta = 4$), the single-photon addition ($k = 1$) yields a CF value of 0.5, while for the higher photon-addition cases (i.e., $k \geq 3$), the quadrupled ratio is sufficient to induce near maximum genuine tripartite entanglement. In particular, for the case where $k = 5$, the CF saturates for $\eta \geq 2$. Hence, for the higher photon-addition cases, the state retains its genuine tripartite entanglement character for the equal noise ratio.

4. Conclusions

In this article, we evaluated the genuine tripartite entanglement present in the three-mode CV states. We showed that the quasi-GHZ and quasi-W states possessed maximum CFs in their respective regimes for higher coherent strength. At lower coherent strength, the states are far from possessing maximum entanglement. The addition of photons in the single-mode and three-mode levels in the quasi-GHZ and quasi-W states leads to an earlier onset of genuine tripartite entanglement. In particular, distributing photons to all the modes would greatly enhance the entanglement rather than adding more photons in a single mode. Furthermore, nonlocal photon addition to a product three-mode coherent state produces W-type genuine tripartite entanglement for higher infused quantum noise through photon addition. Our results indicate that the manipulation of genuine tripartite entanglement in CV radiation states is feasible with photon addition.

References

1. M. A. Neilsen and I. L. Chaung, *Quantum Computation and Quantum Information*, Cambridge Univ. Press, Cambridge, MS (2000).
2. W. K. Wootters, *Phys. Rev. Lett.*, **80**, 2245 (1998).

3. L. Henderson and V. Vedral, *Phys. Rev. Lett.*, **84**, 2263 (2000).
4. Z. H. Ma, Z. H. Chen, J. L. Chen, et al., *Phys. Rev. A.*, **83**, 062325 (2011).
5. Y. Hong, T. Gao, and F. Yan, *Phys. Rev. A.*, **86**, 062323 (2012).
6. B. C. Hiesmayr and M. Huber, *Phys. Rev. A.*, **78**, 012342 (2008).
7. B. Jungnitsch, T. Moroder, and O. Guhne, *Phys. Rev. Lett.*, **106**, 190502 (2011).
8. O. Viehmann, C. Eltschka, and J. Siewert, *Phys. Rev. A.*, **83**, 052330 (2011).
9. A. Osterloh, *J. Math. Phys.*, **50**, 033509 (2009).
10. S. Szalay, *Phys. Rev. A.*, **92**, 042329 (2015).
11. V. Coffman, J. Kundu, and W. K. Wootters, *Phys. Rev. A.*, **61**, 052306 (2000).
12. S. Xie and J. H. Eberly, *Phys. Rev. Lett.*, **127**, 040403 (2021).
13. G. Meng-Li, J. Zhi-Xiang, L. Bo, and F. Shao Ming, *J. Phys. A: Math. Theor.*, **56**, 315302 (2023).
14. T. C. Ralph, *Rep. Prog. Phys.*, **69**, 853 (2006).
15. G. S. Agarwal and K. Tara, *Phys. Rev. A.* **43**, 492 (1991).
16. L. Hong, *Phys. Lett. A.*, **264**, 265 (1999).
17. V. V. Dodonov, Y. A. Korennoy, V. I. Man'ko, and Y. A. Moukhin, *Quantum Semiclass. Opt.*, **8**, 413 (1996).
18. G. Ren and W. Zhang, *Optik*, **181**, 191 (2019).
19. A. Meslouhi, H. Amellal, Y. Hassouni, and A. El Allati, *J. Russ. Laser. Res.*, **35**, 369 (2014).
20. Y. Oulouda, M. El Falaki, and M. Daoud, *J. Russ. Laser. Res.*, **44**, 13 (2023).
21. H. Baba, M. Mansour, and M. Daoud, *J. Russ. Laser. Res.*, **43**, 124 (2022).
22. F. Siyouri, M. Ziane, M. El Baz, and Y. Hassouni, *J. Russ. Laser. Res.*, **38**, 27 (2017).
23. G. Adesso and F. Illuminati, *J. Phys. A: Math. Theor.*, **40**, 7821 (2007).
24. N. Meher and S. Sivakumar, *Quantum Inf. Process.*, **17**, 233 (2018).
25. M. G. A. Paris, *Phys. Rev. A.*, **62**, 033813 (2000).
26. A. Zavatta, S. Viciani, and M. Bellini, *Science*, **306**, 660 (2004).
27. A. Zavatta, S. Viciani, and M. Bellini, *Phys. Rev. A.*, **75**, 052106 (2007).
28. H. M. Li, H. C. Yuan, and H. Y. Fan, *Int. J. Theor. Phys.*, **48**, 2849 (2009).
29. M. Daoud and R. Ahl Laamara, *Open Syst. Inf. Dyn.*, **22**, 1550023 (2015).
30. L. Jebli, R. Houca, and M. Daoud, *Int. J. Theor. Phys.*, **61**, 231 (2022).
31. J. Fiurasek, *Phys. Rev. A.*, **65**, 053818 (2002).
32. S. Y. Lee and H. Nha, *Phys. Rev. A*, **85**, 043816 (2012).
33. Z. Wang and X. Fang, *Optik*, **126**, 1838 (2015).
34. T. M. Duc, T. Q. Dat, and H. S. Chuong, *Int. J. Mod. Phys. B.*, **34**, 2050223 (2020).
35. X. X. Xu and F. S. Xie, *Int. J. Theor. Phys.*, **52**, 2784 (2013).